a

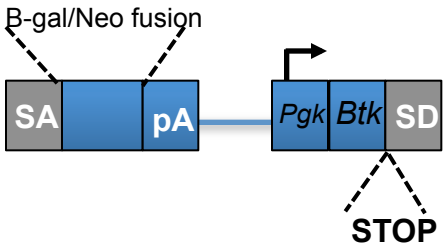

b

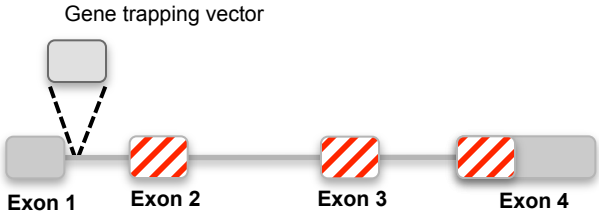

c

GATTAGCTCAGGTTTACATCAGCCGGGCGGGGATCCGAGCCCGCGTCCCGGTGCCGCAGCACTTTAGCA
GCGGAAGAGGCTGCTGCCGAGTACGTGACGGCTGGGGTCTGGCACTAGCGTGCAGGAGACTCCGAGAGC
TGCTCAGTTAGGCTGGCGGCGGTCCACGGGCGTGGGCGCAGGCGGCTCTGAGGCTCCAGGACAAGGTAC
CCAGTAGGGAGCTGCGAAGGGGGATTTACCCGGGTCTGGCAAG*AGGGTCACTGGAAGTCCAGGCGTAT
TCATGAATATTTCTATTCTCTCTCTCTCTCTCTCTCTCTCTCTCTCTCTCTCTCTCTCTCTCTCTCTCT
CTCTCTCGTTCTCTCTCTCTCTCGTTCTCTCCCTCTCGCTCTCGCTCTCTTTTACTCACTCTCACTCTT
CTCACTCTCACTCTCTCGCTCCTTTACTTCGCCGTCTGGGGGCGCCCTCAGCCTGAGCTGTCGACCCCA
GCTTATTATGCAGCCCAG

* =Insertion Site

d

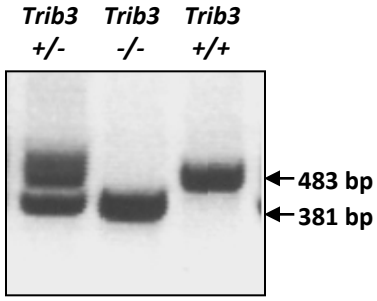

e

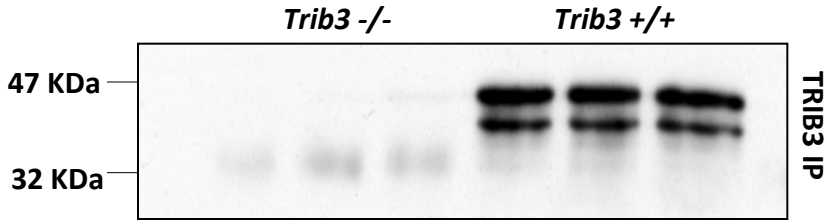

f

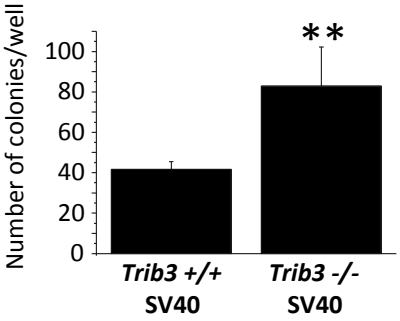

g

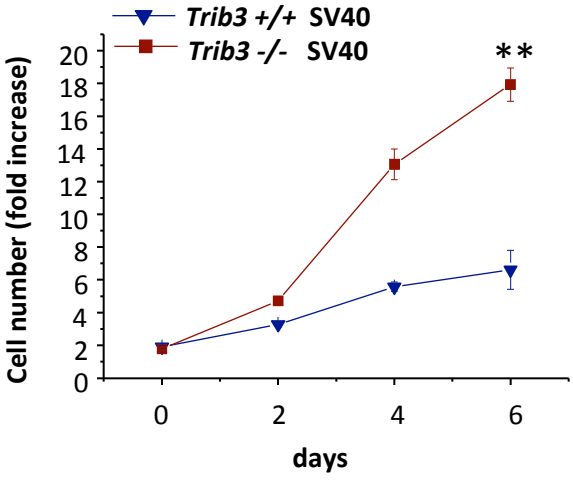

Supplementary Figure S1. Genetic inhibition of TRIB3 facilitates oncogene transformation and enhances the tumorigenicity of transformed embryonic fibroblasts.

(**a-e**) Generation of *Trib3*$^{-/-}$ mice using the gene-trap system. (**a**) The gene trap vector used to inactivate the *Trib3* allele included two expression cassettes. The first cassette encoded for a splice acceptor site (SA), followed by a fusion protein of beta-galactosidase and neomycin, thereby disrupting transcription of the targeted mRNA. The second cassette encoded for a "diagnostic marker", followed by a splice donor site and was used to determine the site of insertion for the targeting vector by 3' RACE. (**b**) Schematic showing the *Trib3* allele, which was targeted in the first intron using the gene-trap vector. (**c**) The sequence includes 250 nucleotides on either side of the insertion site, denoted by an asterisk (data kindly provided by Lexicon Pharmaceuticals). (**d**) PCR amplification (performed on genomic DNA obtained from *Trib3*$^{+/+}$, *Trib3*$^{+/-}$ and *Trib3*$^{-/-}$ mice) of the region where the gene trap vector is inserted (Forward primer hybridizes on *Trib3* exon-1 and reverse primers hybridize on intron 1-2 of the wild type allele and on the 5' region of the gene-trap vector, respectively). (**e**) Insertion of the gene trap vector prevents the expression of the TRIB3 protein. The panel shows TRIB3 protein levels as determined by immunoprecipitation and subsequent Western blot analysis in lysates obtained from cells derived from *Trib3*$^{+/+}$ and *Trib3*$^{-/-}$ animals. (**f**) Effect of the expression of SV-40 T-large antigen on the ability of *Trib3*$^{+/+}$ and *Trib3*$^{-/-}$ MEFs to form colonies in soft agar (cells were transduced with a retroviral vector encoding SV-40 T-large antigen). Data correspond to the number of colonies formed per dish in each experimental condition (mean ± SD; n = 3; $^{**}P < 0.01$ relative to *Trib3*$^{+/+}$ MEFs). (**g**) Effect of the expression of SV-40 T-large antigen on the number of *Trib3*$^{+/+}$ and *Trib3*$^{-/-}$ MEFs after several days in culture. Data correspond to the number of crystal-violet positive cells at each time point relative to the number of cells at day 0 for each experimental condition (mean ± SD; n = 3; $^{**}P < 0.01$ relative to SV40-T large antigen-*Trib3*$^{+/+}$ MEFs).

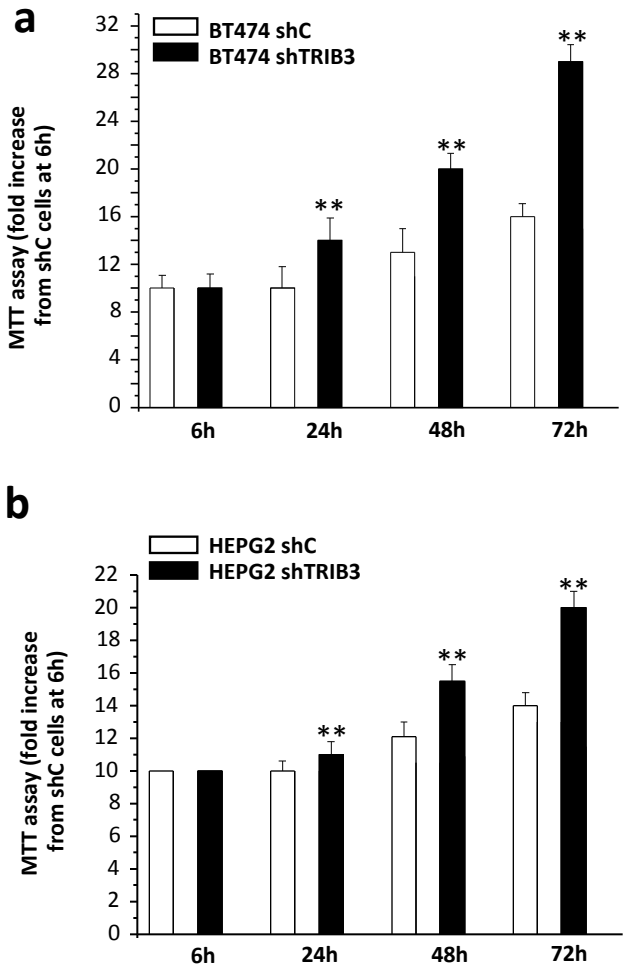

Supplementary Figure S2. Genetic inhibition of TRIB3 enhances the viability of cancer cell lines

Effect of TRIB3 stable knock-down on the number of shC and shTRIB3 BT474 (**a**) and HEPG2 (**b**) cells (as estimated by the MTT test) (mean ± SD; n = 5; ***P* < 0.01 from shC cells at each time point).

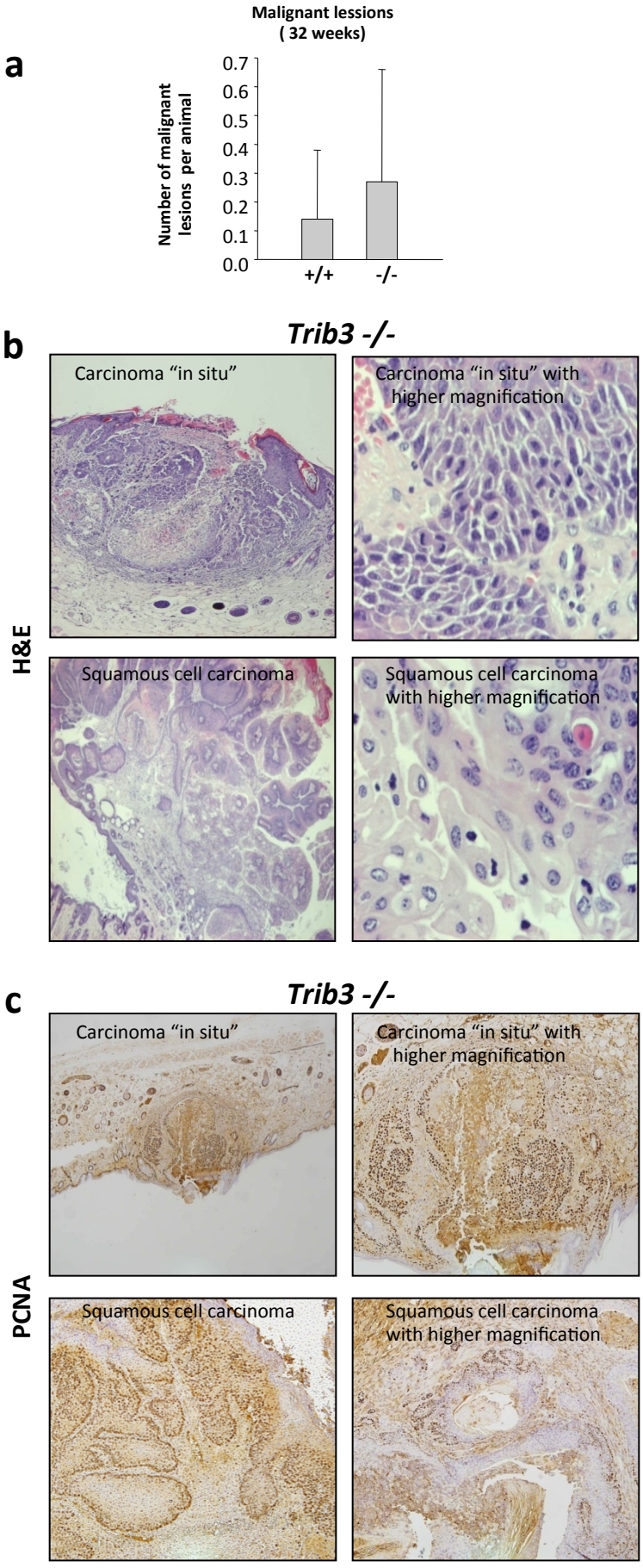
a
Malignant lessions
(32 weeks)
Number of malignant lesions per animal
0.7
0.6
0.5
0.4
0.3
0.2
0.1
0.0
+/+
-/-
b
Trib3 -/-
H&E
Carcinoma "in situ"
Carcinoma "in situ" with higher magnification
Squamous cell carcinoma
Squamous cell carcinoma with higher magnification
c
Trib3 -/-
PCNA
Carcinoma "in situ"
Carcinoma "in situ" with higher magnification
Squamous cell carcinoma
Squamous cell carcinoma with higher magnification

Supplementary Figure S3. Analysis of the effect of TRIB3 genetic deletion on the incidence of mouse skin carcinomas

(**a**) Effect of TRIB3 genetic inactivation on the incidence of skin carcinomas in *Trib3*$^{-/-}$ and *Trib3*$^{+/+}$ mice subjected to the two-stage skin carcinogenesis protocol (animals were sacrificed 20 or 32 weeks after the administration of the DMBA treatment and subsequently subjected to hystopathological analyses). Data are expressed as the mean number of squamous cell carcinomas per animal ± SEM) [7 *Trib3*$^{+/+}$ and 9 *Trib3*$^{-/-}$ mice sacrificed on week 32 were analyzed]. (**b,c**) Representative images of hematoxilin/eosin (**b**, left panels: 2x, right upper panel: 20x and right lower panel: 40x) and PCNA staining (**c**; left panels: 2x; right panels: 10x) of squamous carcinomas or in situ carcinomas observed in *Trib3*$^{-/-}$ mice.

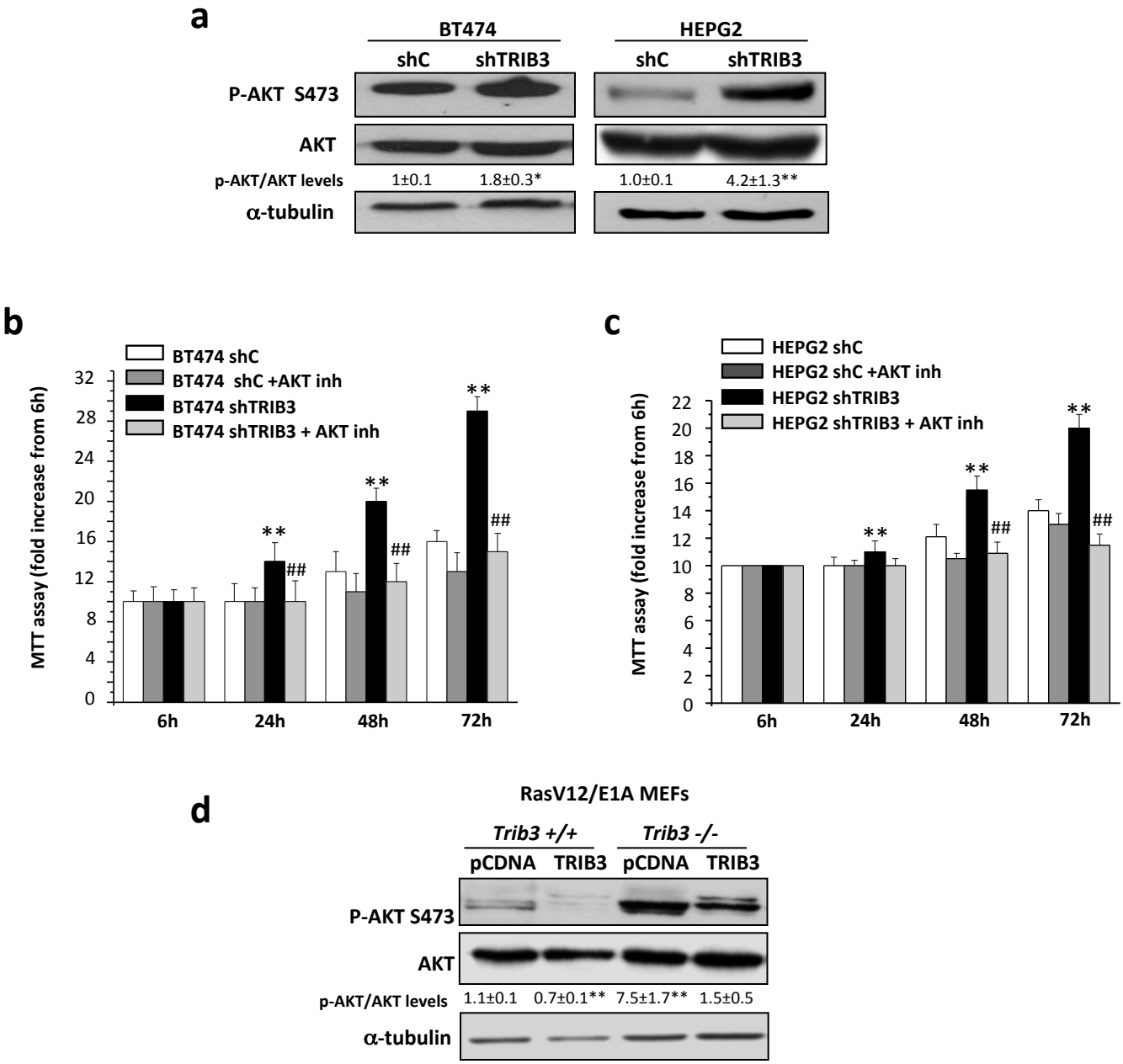

Supplementary Figure S4. Genetic inhibition of TRIB3 enhances the viability of cancer cell lines via AKT

(**a**) Effect of TRIB3 stable knockdown on AKT phosphorylation of BT474 and HepG2 cells (n = 3; a representative Western blot for each cell line is shown). Values in the bottom of each Western blot correspond to the P-AKT/t-AKT ratio and are expressed as the mean fold change ± SD relative to the corresponding shC cells; **P* < 0.05 from shC cells). (**b,c**) Effect of TRIB3 stable knock-down and the AKT inhibitor X (1 μM; 24 h) on the number of BT474 (**b**) and HEPG2 (**c**) cells (as estimated by the MTT test) at the indicated time points (mean ± SD; n = 5; ***P* < 0.01 from shC vehicle-treated cells and ##*P* < 0.01 from shTRIB3 vehicle-treated cells). (**d**) Effect of TRIB3 re-expression on the phosphorylation of AKT on Ser 473 of RasV^{12}/E1A-transformed *Trib3*$^{+/+}$ or *Trib3*$^{-/-}$ MEFs (a representative Western blot analysis is shown). Values in the bottom of the panels correspond to the P-AKT/t-KT ratio and are expressed as the mean fold change ± s.d. relative to pCDNA-transfected, *Trib3*$^{+/+}$ cells [n=3; ** *P* < 0.01 from pCDNA-transfected *Trib3*$^{+/+}$ cells].

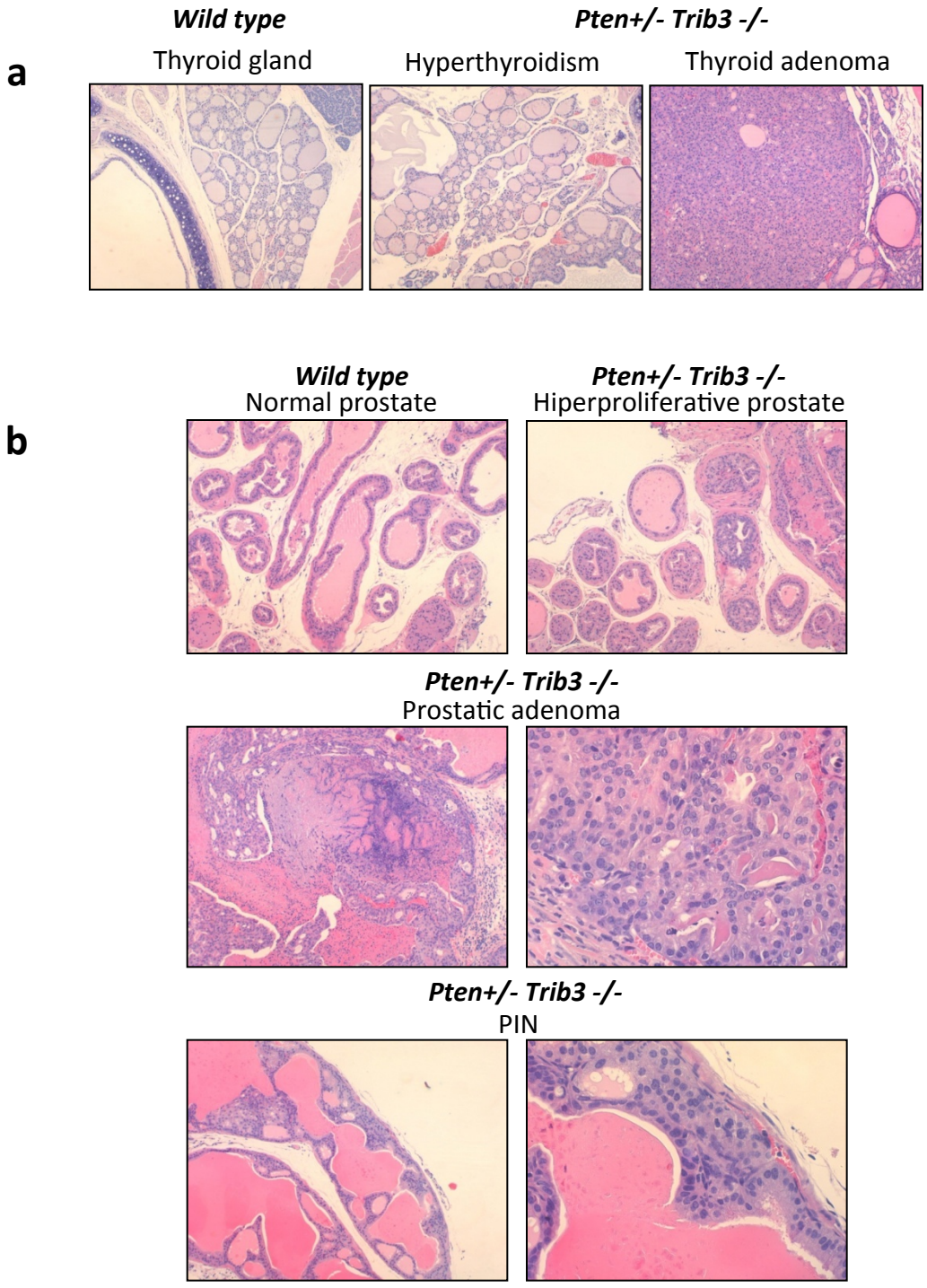

Supplementary Figure S5. Characterization of premalignant and malignant lesions in thyroid and prostate of *Pten*$^{+/-}$ *Trib3*$^{-/-}$ mice

(**a**,**b**) Representative microphotographs of the different lesions observed in the thyroid (**a**: 10x) and the prostate (**b**; upper panels: 10x, middle-lower left panels: 10x and middle-lower right panels: 40x) of *Pten*$^{+/+}$ *Trib3*$^{+/+}$ (WT) and *Pten*$^{+/-}$ *Trib3*$^{-/-}$ animals stained with hematoxilin/eosin.

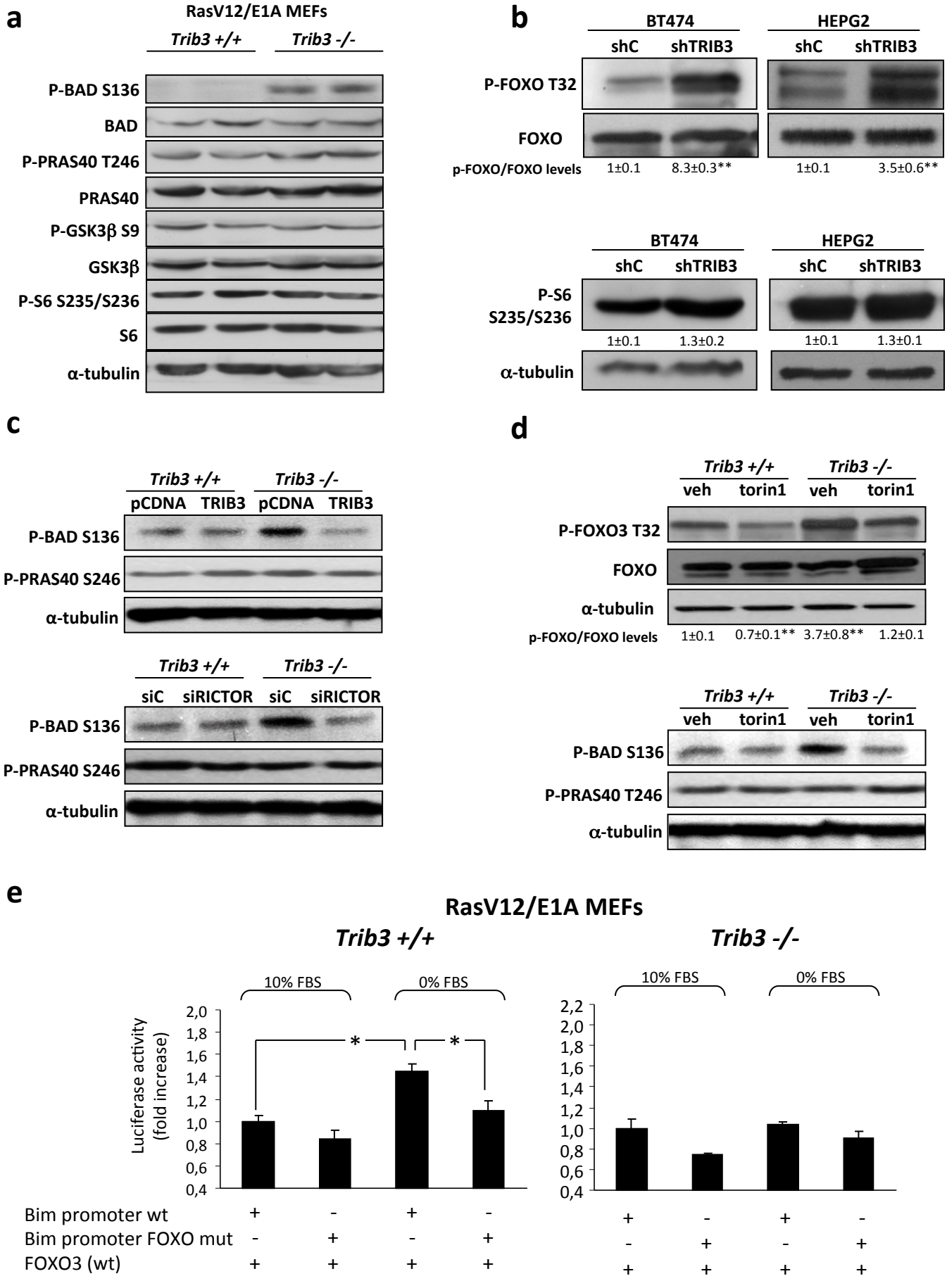
a
RasV12/E1A MEFs
Trib3 +/+
Trib3 -/-
P-BAD S136
BAD
P-PRAS40 T246
PRAS40
P-GSK3β S9
GSK3β
P-S6 S235/S236
S6
α-tubulin
b
BT474
HEPG2
shC
shTRIB3
P-FOXO T32
FOXO
p-FOXO/FOXO levels
1±0.1
8.3±0.3**
1±0.1
3.5±0.6**
P-S6 S235/S236
1±0.1
1.3±0.2
1±0.1
1.3±0.1
α-tubulin
c
Trib3 +/+
Trib3 -/-
pCDNA
TRIB3
P-BAD S136
P-PRAS40 S246
α-tubulin
siC
siRICTOR
d
veh
torin1
P-FOXO3 T32
FOXO
p-FOXO/FOXO levels
1±0.1
0.7±0.1**
3.7±0.8**
1.2±0.1
P-BAD S136
P-PRAS40 T246
e
RasV12/E1A MEFs
Trib3 +/+
Trib3 -/-
10% FBS
0% FBS
Luciferase activity (fold increase)
2,0
1,8
1,6
1,4
1,2
1,0
0,8
0,6
0,4
2,2
*
Bim promoter wt
Bim promoter FOXO mut
FOXO3 (wt)

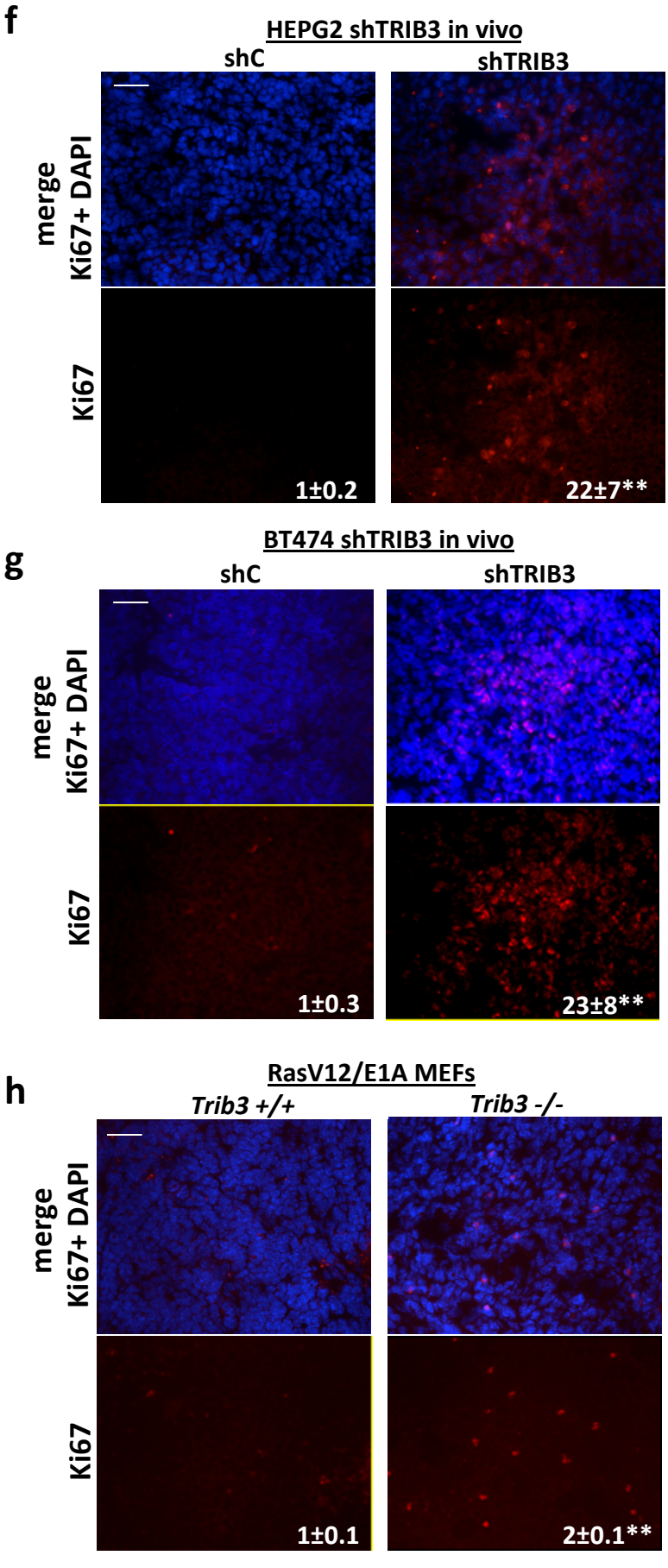
f
HEPG2 shTRIB3 in vivo
shC
shTRIB3
merge
Ki67+ DAPI
Ki67
1±0.2
22±7**
g
BT474 shTRIB3 in vivo
shC
shTRIB3
merge
Ki67+ DAPI
Ki67
1±0.3
23±8**
h
RasV12/E1A MEFs
Trib3 +/+
Trib3 -/-
merge
Ki67+ DAPI
Ki67
1±0.1
2±0.1**

Supplementary Figure S6. Genetic inhibition of TRIB3 enhances the proliferation of cancer cell lines via AKT-dependent FOXO activation.

(**a**) Effect of TRIB3 genetic inactivation on the phosphorylation of BAD, PRAS40, GSK3 and S6 of Ras^{V12}/E1A-transformed MEFs (n=8; a representative experiment is shown). (**b**) Effect of TRIB3 stable knockdown on FOXO (upper panel) and S6 (lower panel) phosphorylation of BT474 and HepG2 cells (n=3; a representative Western blot for each cell line is shown). Values below the Western blots correspond to the densitometric analysis of the P-FOXO/t-FOXO levels (upper panel) or of the P-S6 levels with respect the loading control and are expressed as the mean fold change ± SD relative to the corresponding shC cells; $^{**}P < 0.01$ from shC cells). (**c**) Effect of TRIB3 re-expression (upper panel), and RICTOR knock-down (lower panel) on the phosphorylation of BAD and PRAS40 of $RasV^{12}$/E1A-transformed $Trib3^{+/+}$ and $Trib3^{-/-}$ MEFs (n=3; representative experiments are shown). RICTOR mRNA levels (as determined by real-time quantitative PCR) were reduced by 87±4 % in siRICTOR-transfected cells with respect to the levels of this mRNA in siC-transfected cells). (**d**) Effect of torin1 treatment (250nM, 18h) on the phosphorylation of FOXO (upper panel), BAD and PRAS 40 (lower panel) of $RasV^{12}$/E1A-transformed $Trib3^{+/+}$ and $Trib3^{-/-}$ MEFs. Upper panel: values below the Western blot correspond to the densitometric analysis of the ratio P-FOXO/t-FOXO and are expressed as the mean fold change ± s.d. relative to vehicle-treated (veh) $Trib3^{+/+}$ cells. (n=3; ** $P < 0.01$ from $Trib3^{+/+}$ cells) Lower panel: n=3; a representative experiment is shown. (**e**) Effect of serum withdrawal on the activity of the *Bim* promoter of $RasV^{12}$/E1A-transformed $Trib3^{+/+}$ and $Trib3^{-/-}$ MEFs transfected with a vector encoding FOXO wild type and co-transfected with a luciferase reporter vector containing the sequence of the *Bim* promoter [wild type (wt) or mutated on the FOXO binding sites]. Data correspond to luciferase activity and are expressed as the mean fold change ± SD relative to the corresponding *Bim* promoter (wt)-transfected cells incubated in the presence of serum (n = 4; $^{*}P < 0.05$ from serum-starved, *Bim* promoter (wt)- and FOXO3 (wt)-transfected cells). (**f-h**) Effect of TRIB3 stable knockdown or TRIB3 genetic inhibition on proliferation (as determined by Ki67 immunostaining) of tumor xenografts generated by subcutaneous injection of HepG2 cells (**f**) BT474 cells (**g**) and $RasV^{12}$/E1A-transformed MEFs (**h**) in nude mice. For the immunostaining, values in the lower right corner of each panel correspond to the Ki67-positive cells normalized to the total number of nuclei in each section and are expressed as the mean fold change ± SD relative to control tumors (18 sections for each of 3 dissected tumors for each condition were analyzed; $^{**}P < 0.01$ from tumors generated with control cells).

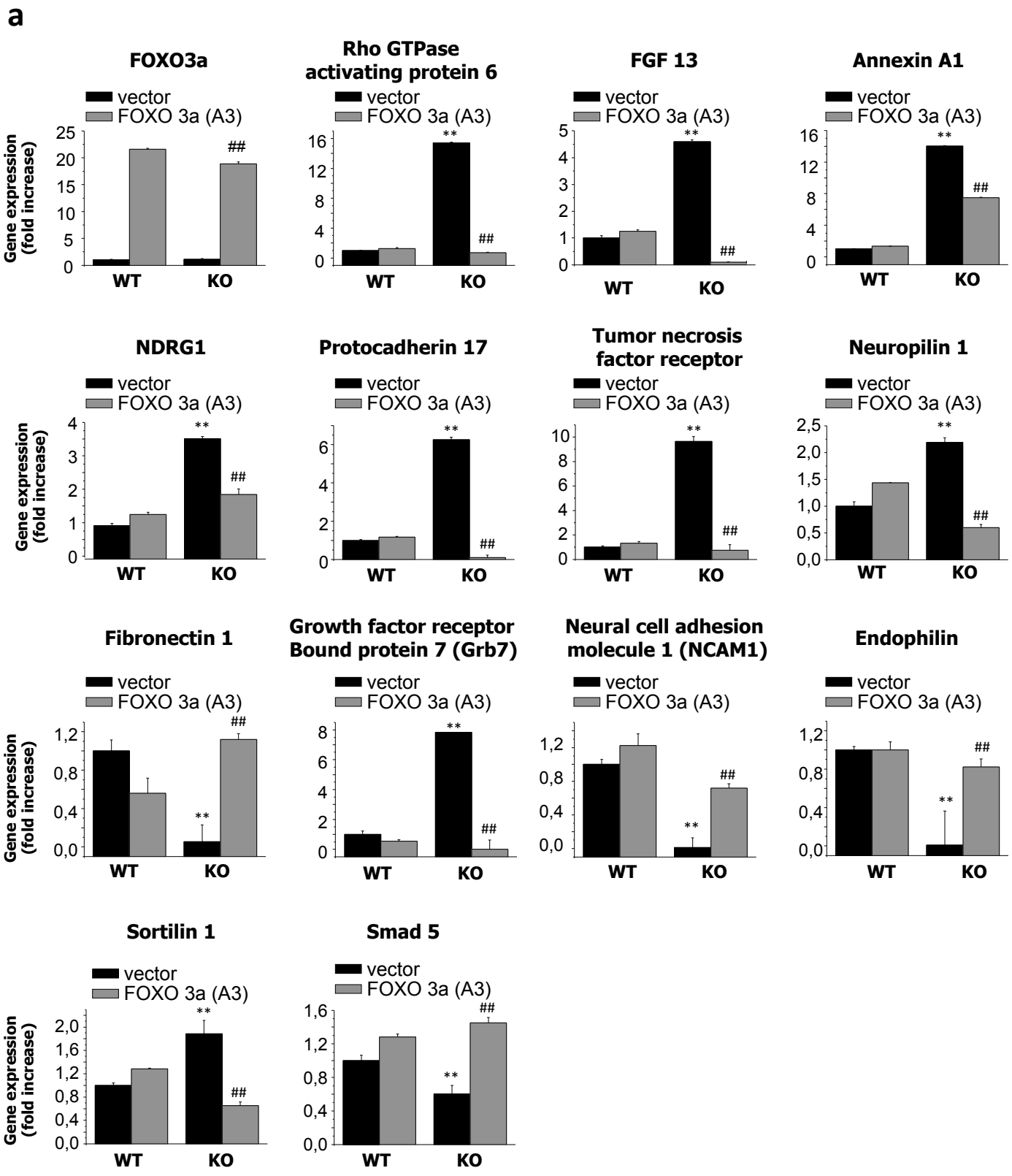
a
FOXO3a
Rho GTPase activating protein 6
FGF 13
Annexin A1
NDRG1
Protocadherin 17
Tumor necrosis factor receptor
Neuropilin 1
Fibronectin 1
Growth factor receptor Bound protein 7 (Grb7)
Neural cell adhesion molecule 1 (NCAM1)
Endophilin
Sortilin 1
Smad 5
vector
FOXO 3a (A3)
Gene expression (fold increase)
WT
KO
**
##

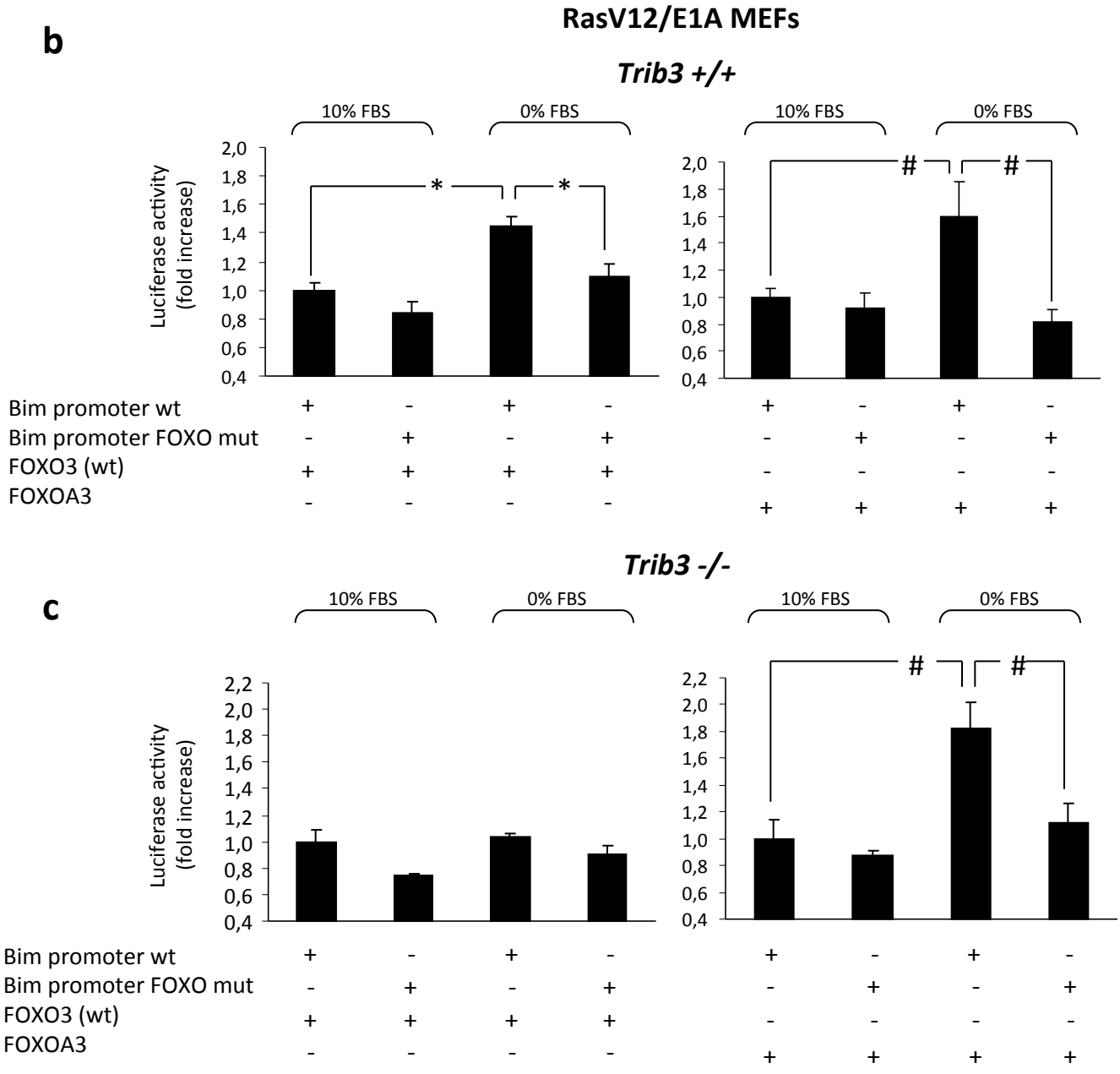

Supplementary Figure S7. Loss of TRIB3 abrogates the FOXO-dependent activation of the *Bim* promoter in response to serum withdrawal

(**a**) Effect of TRIB3 genetic inactivation and stable expression of FOXOA3 on mRNA levels of different genes (as determined by real-time quantitative PCR) of RasV^{12}/E1A-transformed Trib3$^{-/-}$ MEFs (mean fold change relative to pBABE-*Trib3*$^{+/+}$ cells ± SD; n=3; ***P* < 0.01 from pBABE *Trib3*$^{+/+}$ cells ; $^{\#\#}$*P* < 0.01 from pBABE-*Trib3*$^{-/-}$ cells). (**b,c**) Effect of serum withdrawal on the activity of the *Bim* promoter of RasV^{12}/E1A-transformed *Trib3*$^{+/+}$ (**b**) and *Trib3*$^{-/-}$ (**c**) MEFs transfected with a vector encoding FOXO wild type or FOXOA3 and co-transfected with a luciferase reporter vector containing the sequence of the *Bim* promoter [wild type (wt) or mutated on the FOXO binding sites]. Data correspond to luciferase activity and are expressed as the mean fold change ± SD relative to the corresponding *Bim* promoter (wt)-transfected cells incubated in the presence of serum (n = 4; **P* < 0.05 from serum-starved, *Bim* promoter (wt)- and FOXO3 (wt)-transfected cells and $^{\#}$*P* < 0.05 from serum-starved, *Bim* promoter (wt)- and FOXOA3-transfected cells).